Structural basis of multistationary quantum systems. I. Effective single-particle dynamics

K. Obermayer, W. G. Teich, and G. Mahler
Institut für Theoretische Physik, Universität Stuttgart, Pfaffenwaldring 57, 7000 Stuttgart 80, Federal Republic of Germany
(Received 12 August 1987; revised manuscript received 14 December 1987)

The structural basis of multistationarity is discussed on the basis of semiconductor heterostructures on a nanometer scale. It is shown that for an appropriate choice of the system's parameters the microscopic degrees of freedom decouple into "dynamical" and "passive" degrees of freedom, which in turn give rise to multistationary quasimolecular subsystems. Separation of time scales and the selection rules for the pertinent electronic transitions are shown to be controlled by the localization behavior of the electron wave function and thus, finally, by geometrical and band-gap parameters of the semiconductor heterostructure. Selective coupling of discrete electronic eigenstates via local operators (acoustic phonon, dipole interaction) leads to a "switching" dynamics realized by electronic single-particle transitions. Three types of attractors can be distinguished and may be prepared by single modes of the electromagnetic field. The principle uncertainty and the stochastic nature of the quantum-mechanical dynamics are discussed within the context of simple logical operations and the storage of information in quantum systems.

I. INTRODUCTION

The technology and architecture of information-processing systems led to a drastic miniaturization of the hardward elements by several orders of magnitude. While the length of a vacuum tube in 1940 was about 10 cm, the typical length of a transistor on a silicon chip has been reduced to 10 μm in the year 1980 and to 1 μm in the VLSI circuits of today. By direct extrapolation one concludes that the "nanometer chip" containing computing elements of the size of individual molecules will be developed at the beginning of the next century. Does this kind of extrapolation make sense in useful technological terms? Or does there exist an inherent length scale, below which the constraints imposed on systems capable of information processing must violate physical laws?[1]

Open physical systems capable of information processing may be characterized by their repertoire of (addressable) stationary states. This holds for present-day electronic devices, the repertoire of which consists of various current distributions on given networks. Switching in this kind of multistable systems is performed, e.g., by changing the voltage at certain vertices. In the last few years there have been several proposals for alternative concepts.[2-6] A kind of "molecular electronics" could be based, e.g., on polymer chains, for which the switching may involve nonlinear dynamics (solitons or solitary excitations[6-8]). Switching has been shown to occur in molecules in terms of proton[9,10] and electron transfer.[11-13] As opposed to conventional electronics and also to conventional optical bistability, these states do not involve any current (and therefore no battery), but at the same time will keep the switched position only during a limited time, τ_d. In this investigation we will restrict ourselves to electron transfer processes. They are generally fast, easy to prepare and to detect; furthermore, the change in a local charge distribution can be used to incorporate interactions between multistationary subsystems, as will be discussed in the second part of our work.[14]

A solid is a typical many-body system, the dynamics of which is generally described by collective processes. Quasimolecular (i.e., few-body) subsystems can be obtained only if the solid-state material has a nanometer- or subnanometer-scale microstructure. These include the generation of localized electronic states due to impurities or lattice defects[15-17] and the confinement of electrons and holes in localized electronic states of semiconductor quantum "dots."[18,19] Castro *et al.*,[15] Bjorklund *et al.*,[16] and Moerner and Levenson[17] proposed "molecular" optical storage elements on the basis of persistent hole burning (PHB) into the inhomogeneously broadened absorption lines of impurity spectra in solids. PHB elements have the disadvantage that the spatial localization of the elements, their spectrum, and the selection rules for electronic transitions cannot be controlled during the manufacturing process. Therefore it would be quite difficult to construct more complex systems capable of performing, e.g., simple logical operations or even repeated read-write operations on an equivalent time scale. Semiconductor quantum dots, on the other hand, may provide a more "flexible" material. Their spectrum and their selection rules depend on the geometrical parameters of the heterostructure which, in principle, can be varied within rather broad limits. Preliminary results have been given in Refs. 18 and 19 and reviewed in Ref. 20.

Our aim is to describe specific multistable quantum systems and their surroundings within a microscopic model based on physically realistic materials and interactions. This allows a detailed discussion not only of the

switching dynamics, but also of the preparation process and the role of "external" degrees of freedom. Although the reference to specific interactions may seem a less "general" approach, compared with previous investigations of the physical foundations of information processing,[1,21–26] it has several advantages.

(1) It offers the possibility of discussing constraints arising from the fact that there are only a limited number of basic (microscopic) types of interactions realized in nature. This may be seen as a complementary approach to the search for "minimal" dynamical models[27,28] which are consistent with the formalism of classical or quantum mechanics and are capable of processing information.

(2) It allows the investigation of the question how multistationarity and complex dynamics can be achieved. This is especially challenging for systems with only a few degrees of freedom.

(3) It may lead to experimentally testable consequences.

This paper presents the first part of our work. Here we are mainly concerned with the physical realization of multistationarity and the coupling to the preparation system, the measurement system, and the surroundings. We will investigate systems with switching states connected by single-electron transitions, where an (effective) single-particle theory is sufficient. In the present case, effective single-particle dynamics should thus not only mean (approximate) independent-particle behavior, but, furthermore, a reduction of the relevant state space to states which differ by just a single electron transfer excitation. More general switching dynamics, which makes use of several interacting electrons, and the physical realization of logical operations will be the topic of the following paper.[14]

This first part is organized as follows: Section II will be concerned with the separation of the microscopic degrees of freedom into "dynamical" and "passive" degrees of freedom, resulting from a separation of time scales for different pathways in the system's state space. As an example, we will treat a three-dimensional semiconductor heterostructure on a nanometer scale. In Sec. III we will shortly present our concept of multistability in open quantum systems and introduce some terms used in the following discussion. The switching dynamics of an elementary multistationary system and the coupling to the preparation and the measurement system will be discussed within a quantum optical model in Sec. IV. In Sec. V, finally, we investigate some consequences for elementary "single electron" information processes.

II. HIERARCHICAL STRUCTURES AND DECOUPLING OF STATE SPACES

A. Spectrum and eigenfunctions

Figure 1 shows the real-space model structure of a single multistable element as proposed in Ref. 18. We describe the model structure by a simple effective-mass envelope-function model[29,30] for each band. For isolated bands the one-particle wave function $\phi_{n\mathbf{k}}(\mathbf{r})$ near the band edge is split into a slowly varying envelope function

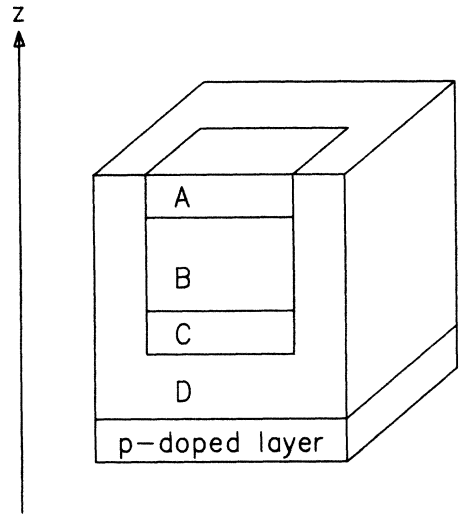

FIG. 1. Real-space model structure of a single multistable element. Three blocks of different semiconductor materials A, B, and C and with width S in the x-y direction are embedded into a coating material D. A p-doped layer serves as a source for holes.

$\psi_{n\mathbf{k}}(\mathbf{r})$ and the Bloch function $u_{n0}(\mathbf{r})$ at the band edge:

$$\phi_{n\mathbf{k}}(\mathbf{r})=b\psi_{n\mathbf{k}}(\mathbf{r})u_{n0}(\mathbf{r}) , \tag{2.1}$$

where b is an appropriate normalizing constant. The envelope functions $\psi_{n\mathbf{k}}(\mathbf{r})$ are nearly constant within a unit cell and satisfy the effective-mass equation

$$\left[-\frac{\hbar^2}{2m_{nj}^*}\Delta+U(\mathbf{r})\right]\psi_{n\mathbf{k}}^j(\mathbf{r})=(E_{n\mathbf{k}}-E_n^j)\psi_{n\mathbf{k}}^j(\mathbf{r}) \tag{2.2}$$

within each semiconductor material j. $\psi_{n\mathbf{k}}^j(\mathbf{r})$ denotes the envelope function for a quasiparticle in the band n with momentum $\mathbf{k}$, E_n^j denotes the bulk band-edge energy, and m_{nj}^* the effective mass within the material j, and $U(\mathbf{r})$ is a slowly varying external potential, e.g., a space-charge potential or a Hartree term. The interfaces between the three central blocks are modeled by abrupt steps.

Figure 2 shows spectrum and eigenfunctions for the lowest-lying conduction-band (CB) and valence-band (VB) states of a double-quantum-dot model structure for different band-gap parameters (for details of the calculation see Appendix A). The electronic spectrum consists of a discrete section, characterized by the quantum numbers k_x, k_y, and κ. The envelope functions for the CB and VB states in a single quantum dot (same materials A, B, and C) are both delocalized over the whole structure [Fig. 2(a)]. An additional structuring of the CB and VB band edges leads to localized VB states, while the CB states are still delocalized over the quantum dot [Figs. 2(b)–2(d)]. This effect is most distinct for a small band-offset parameter β [Fig. 2(b)], but could be realized for a higher band-offset parameter, too, if the difference between the effective CB and VB masses is sufficiently high [Fig. 2(c)]. Within the pertinent model structure β describes the ratio between the CB and VB discontinuities

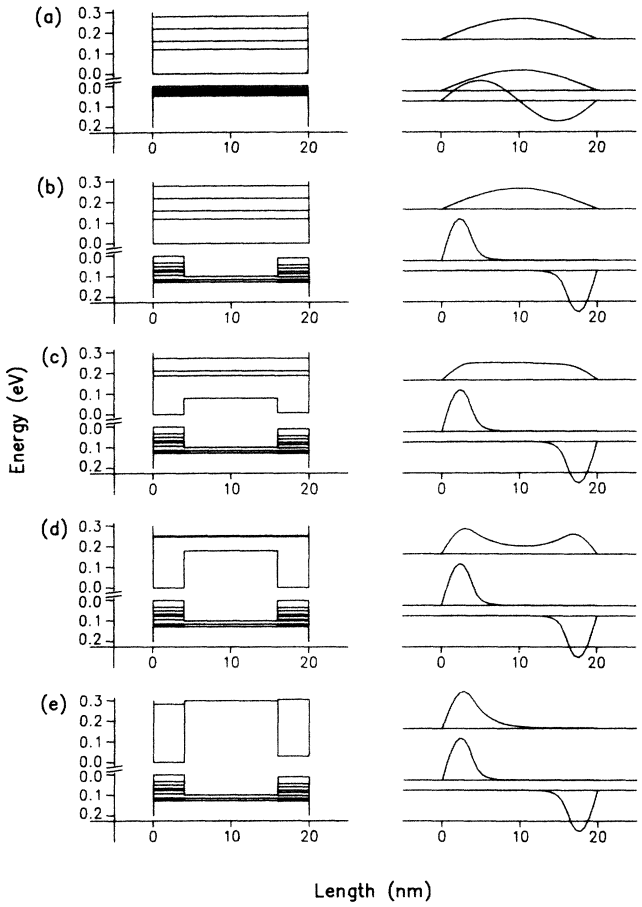

FIG. 2. Spectrum and envelope functions for different band-gap parameters. The figures on the left show the (bulk) VB and CB edges ("double-well potential") and the discrete energy levels near the band edge. The localization behavior of the envelope function is indicated by the length of the horizontal bars. In the VB the discrete electronic states below the band edge of material B are not resolved. The figures on the right side show the envelope functions of the two highest VB states and the lowest CB state, respectively. The parameters of the model structures are $d_A=4$ nm, $d_B=12$ nm, $d_C=4$ nm, and (a) $E_{VB}^A=0$ meV, $E_{VB}^B=0$ meV, $E_{VB}^C=0$ meV, $\beta=0$; (b) $E_{VB}^A=0$ meV, $E_{VB}^B=100$ meV, $E_{VB}^C=10$ meV, $\beta=0$; (c) $E_{VB}^A=0$ meV, $E_{VB}^B=100$ meV, $E_{VB}^C=10$ meV, $\beta=0.8$; (d) $E_{VB}^A=0$ meV, $E_{VB}^B=100$ meV, $E_{VB}^C=1$ meV, $\beta=1.8$; (e) $E_{VB}^A=0$ meV, $E_{VB}^B=100$ meV, $E_{VB}^C=10$ meV, $\beta=3$.

$\beta=(E_{CB}^A-E_{CB}^j)/(E_{VB}^A-E_{VB}^j)$, which we have set equal for the materials $j=B,C$. A small effective mass of the CB electrons leads to a high kinetic energy and therefore to a much lower "effective barrier" $E_n^B-[E_{n\kappa}-E_n^B(k_x,k_y)]$ within the CB than within the VB and is responsible for the different localization behavior. Different localization behavior for a high band-offset parameter occurs only within a small range of the geometrical and band-gap parameters and is a resonance effect [Figs. 2(d) and 2(e)].

The electronic subsystem must now be coupled to other degrees of freedom of the heterostructure and its surroundings. Neglecting correlations, this can be done by describing the surroundings as external reservoirs: "matter" reservoirs (e.g., the phonon system) and the photon-field reservoir (vacuum). Coupling to these reservoirs leads to transitions between the electronic eigenstates of the heterostructure: interband transitions, interwell transitions (i.e., transitions between eigenstates with different localization behavior within the same band), and intrawell transitions. In the following we will show that the different types of localization are the structural basis for largely different time scales.

B. Time scales

Interband transitions define the relaxation time τ_r. For direct semiconductors with a large band gap, τ_r is determined by optical decay. For the transition probability of a spontaneous electronic transition from a (discrete) CB level into an unoccupied (discrete) VB level we get[31]

$$w_{n\mathbf{k},n'\mathbf{k}'}^{\text{opt}}=\frac{\hbar e^2\omega}{16\pi^2\epsilon_0 m^2c^3}\sum_{\nu=1}^{2}\int |M_{n\mathbf{k},n'\mathbf{k}',q\nu}^{\text{opt}}|^2 d\Omega\ , \tag{2.3}$$

$$M_{n\mathbf{k},n'\mathbf{k}',q\nu}^{\text{opt}}=\langle\phi_{n\mathbf{k}}|e^{i\mathbf{q}\cdot\mathbf{r}}\mathbf{e}_{q\nu}\cdot\nabla|\phi_{n'\mathbf{k}'}\rangle\ , \tag{2.4}$$

where ω denotes the resonant transition frequency between the initial and the final state and $\mathbf{e}_{q\nu}$ denotes the polarization vector of the light mode with momentum $\mathbf{q}$. As shown in Appendix B, Eq. (2.4) is controlled by the overlap integral:

$$w_{n\mathbf{k},n'\mathbf{k}'}^{\text{opt}}\propto\left|\int\chi_{n\kappa}^*\chi_{n'\kappa'}dz\right|^2\ , \tag{2.5}$$

where $\chi_{n\kappa}(z)$ describes the z dependence of the envelope function (cf. Appendix A).

The corresponding time scale for the inter well processes, the relaxation time τ_d, is determined by electron-phonon scattering processes and can be estimated by considering the first-order intraband deformation-potential scattering by longitudinal-acoustic (bulk) phonons for the VB states. This will give the appropriate time scale for low-temperature and acoustically-well-matched materials, when optical-phonon scattering and scattering by slab and interface modes can be neglected. The transition probability for a phonon-induced transition is given by[32]

$$w_{n\mathbf{k},n\mathbf{k}'}^{\text{ph}}=\frac{D_1^2}{8\pi^2\rho v}\int_{\text{BZ}}q[n(\mathbf{q})+\tfrac{1}{2}\mp\tfrac{1}{2}]\,|M_{n\mathbf{k},n\mathbf{k}',\mathbf{q}}^{\text{ph}}|^2$$
$$\times\delta(E_{n\mathbf{k}}-E_{n\mathbf{k}'}\pm\hbar vq)d^3q \tag{2.6}$$

$$M_{n\mathbf{k},n\mathbf{k}',\mathbf{q}}^{\text{ph}}=\langle\phi_{n\mathbf{k}}|e^{i\mathbf{q}\cdot\mathbf{r}}|\phi_{n\mathbf{k}'}\rangle\ , \tag{2.7}$$

where ρ denotes the density, v the sound velocity, D_1 the deformation potential, $\mathbf{q}$ the phonon momentum, and $n(\mathbf{q})$ the Bose-Einstein distribution for the occupation of the phonon modes. The integral is over the first Brillouin zone (BZ). The upper sign corresponds to phonon absorption and the lower sign to phonon emission processes. We assume equal density, sound velocity, and deformation potential within the whole heterostructure and we use the long-wavelength limit $\omega=vq$ of the dispersion re-

lation. Again (cf. Appendix C), the transition rate is found to be (approximately) controlled by an overlap integral:

$$w^{\mathrm{ph}}_{n\mathbf{k},n\mathbf{k}'} \propto \left[\int |\chi^{*}_{n\kappa}| \, |\chi_{n\kappa'}| \, dz\right]^2 . \tag{2.8}$$

Figure 3 shows the overlap integrals according to Eq. (2.5) and (2.8) between the highest VB states (1 and 2) and the lowest CB state (3), depending on selected geometrical parameters of a model heterostructure. For small values of the parameters d_B, E^B_{VB}, $d_{A,C}$, and $E^A_{\mathrm{VB}} - E^C_{\mathrm{VB}}$ the selection rules are determined by symmetry, especially for $d_{A,C}=0$ and $E^A_{\mathrm{VB}} - E^C_{\mathrm{VB}}=0$, where the whole structure has reflection symmetry with respect to a plane in the middle of the barrier B. Transition 3-1 is allowed, since both envelope functions are symmetrical, while the transition 3-2 is forbidden. For $d_B=0$ and $E^B_{\mathrm{VB}}=0$ the symmetry is slightly broken, but the influence of the symmetry selection rule is still visible. Going to higher values of the shown parameters, the effective barrier increases, which leads to an increased localization of the envelope functions. Therefore integral 3-1 increases, while the integrals 3-2 and 2-1 decrease. Due to the different effective masses, the VB states will be localized for much smaller values of the parameters than the CB states. This leads to a parameter window where one may achieve a difference of several orders of magnitude between the overlap integrals 3-1 and 3-2 (equal magnitude) and the overlap integral 2-1. Contrary to the selection rules for transitions in atoms and molecules, the selection rules (2.5) and (2.8) for transitions within a complex heterostructure are in general not determined by symmetry, but by the spatial localization behavior of the envelope functions. It will be shown in the next section that such a time-scale spreading is a prerequisite for multistability.

Table I shows the transition rates (2.3) and (2.6) for the parameters of a specific material, the ternary semiconductor $Ga_{1-x}Al_xAs$ (for details of the calculation see Appendixes B and C). Due to the selection rules (2.5) and (2.8), the transitions 3-1 and 3-2 are allowed, while transition 2-1 is forbidden for the pertinent choice of the geometrical parameters and the Al concentration. While the transition rates are very sensitive to changes in the parameters describing the band-gap structure in the z direction, the length in the x and y directions does not severely change the relaxation rates 3-1, 3-2, and 2-1. The interwell scattering rate between electronic eigenstates deeper in the VB is, of course, much greater than the scattering rate 2-1. This is especially true for transitions between eigenstates with light-hole character. Since they must be described by a much lower effective mass, the corresponding envelope function is much more delocalized, and the scattering rates are comparable with or shorter than the optical decay time (depending on geometrical and band-gap parameters). If the double quantum dot has trapped just one hole, the contribution of the light-hole states and the more delocalized heavy-hole states to the total scattering rate between the two VB wells decreases exponentially for low temperatures. In the limit $T \to 0$ K it will be zero, since then all excited VB states are unoccupied.

Up to now, time-scale spreading has been discussed for a semiconductor system with high band-offset parameter [$Ga_{1-x}Al_xAs$ is likely to be an example, $1<\beta<6$ (Refs.

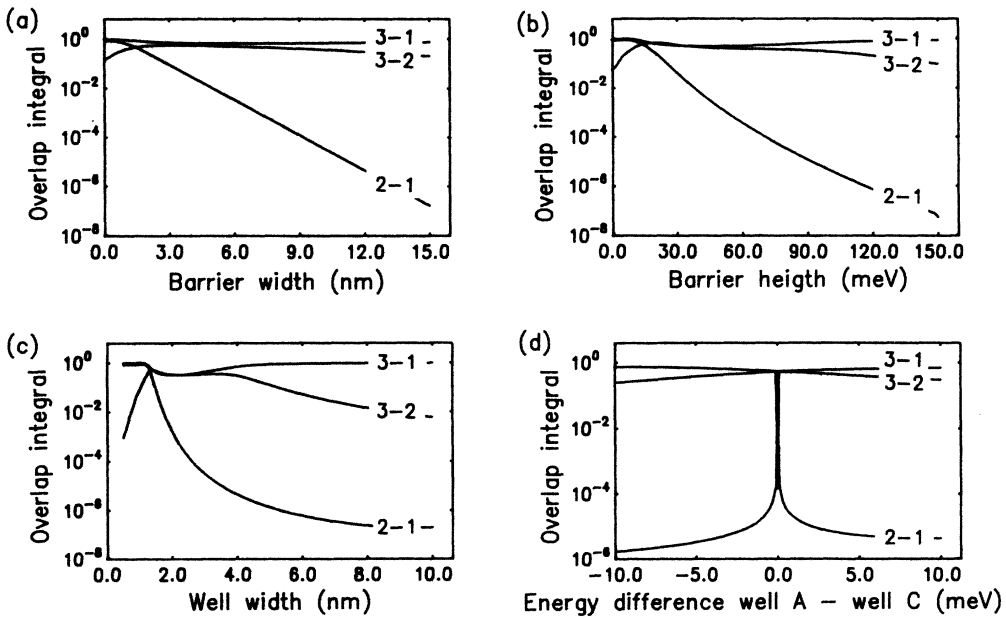

FIG. 3. Overlap integrals as a function of geometrical and band-gap parameters. 1 and 2 denote the highest VB and 3 the lowest CB state, respectively. Shown are the overlap integrals as a function of (a) the barrier width (parameters: $d_A=d_C=4$ nm, $E^A_{\mathrm{VB}}=0$ meV, $E^B_{\mathrm{VB}}=100$ meV, $E^C_{\mathrm{VB}}=10$ meV, and $\beta=1.5$); (b) the barrier height E^B_{VB} (parameters: $d_A=d_C=4$ nm, $d_B=12$ nm, $E^A_{\mathrm{VB}}=0$ meV, $E^C_{\mathrm{VB}}=10$ meV, and $\beta=1.5$); (c) the well width $d_A=d_C$. (parameters: $d_B=12$ nm, $E^A_{\mathrm{VB}}=0$ meV, $E^B_{\mathrm{VB}}=100$ meV, $E^C_{\mathrm{VB}}=10$ meV, and $\beta=1.5$); (d) the well-A–well-C energy difference ($E^C_{\mathrm{VB}}-E^A_{\mathrm{VB}}$). (parameters: $d_A=d_C=4$ nm, $d_B=12$ nm, $E^A_{\mathrm{VB}}=0$ meV, $E^B_{\mathrm{VB}}=100$ meV, and $\beta=1.5$).

TABLE I. Rates in units of s^{-1} for the transitions 3-1 and 3-2 and the transition 2-1 in a quantum dot structure, realized within the $Ga_{1-x}Al_xAs$ system with bandgap offset β. For a rough estimate of the time scales, the transition rates are given for interband transitions with spontaneous emission of photons ($3\rightarrow 1, 3\rightarrow 2$) and for intraband transitions under emission of acoustical phonons ($2\rightarrow 1$). The geometrical and band-gap parameters are $d_A = d_C = 4$ nm, $d_B = 12$ nm, $x_A = 0$, $x_B = 0.2$, $x_C = 0.01$, and $T = 10$ K. S is the quantum-dot width in the x-y directions. Material parameters are taken from Refs. 33 and 34.

β	3-1	3-2	2-1
	$S = 10$ nm		
1.0	4×10^7	3×10^7	4×10^{-2}
1.5	7×10^7	3×10^7	4
2.0	1×10^8	3×10^7	130
	$S = 20$ nm		
1.0	4×10^7	3×10^7	1×10^{-2}
1.5	7×10^7	3×10^7	0.8
2.0	1×10^8	3×10^7	33

35–37)]. In heterostructures of this kind the occurrence of spreading critically depends on the large difference in the effective masses between the electron and heavy-hole states. Semiconductor materials with a lower band offset, on the other hand, are much better suited: Time-scale spreading may be feasible in this case even for equal effective masses, since a high barrier within the VB leads to confined VB states, while the much lower barrier in the CB would not destroy the delocalization of the envelope function.

We note in passing that similar relaxation dynamics can be realized also by means of macromolecules.[11–13] Though these materials are less well characterized right now, they offer an interesting alternative to the manufacturing process: Approaching molecular length scales, the difficulties with present days structuring techniques (e.g., electron beams combined with masks) may become prohibitive, so that direct chemical synthesis could be preferable. Furthermore, the quasi-linear chain molecules offer new possibilities as regards to connectivity and topology.

III. MULTISTABILITY AND SWITCHING IN OPEN QUANTUM SYSTEMS

In the last section we have introduced a specific structure model implying different classes of localized states which, in turn, give raise to different time scales in the relaxation behavior within the electronic subspace. We are now going to show that this behavior gives rise to multistability and can be exploited for switching processes if the quantum system is coupled to an appropriate preparation device. For this purpose we consider the dynamics of an open quantum system I, described by a Hamiltonian $\hat{H}_0$ and the coupling to surrounding reservoirs. $\hat{H}_0$ is defined to act on a small, selected subspace of the total state space describing the many-particle system of the nanostructure solid-state system. Each state of the quantum system I is specified by a reduced density matrix $\hat{\rho}$, and its motion in state space (which is spanned, e.g., by the independent elements of the reduced density matrix) is governed by a generalized master equation:[38]

$$\frac{d\hat{\rho}}{dt} = -\frac{i}{\hbar}[\hat{H}_0,\hat{\rho}] + \left.\frac{d\hat{\rho}}{dt}\right|_{\text{incoh}} . \tag{3.1}$$

The last term, the incoherent motion, is usually responsible for the irreversible decay of any initial state into the thermal equilibrium state, defined by the reservoir parameters. This asymptotic limit, however, does not exclude more complex behavior on shorter time scales: The quantum system I will be said to exhibit multistationarity on a time scale $t \ll \tau_d$, if there is a set of states $\hat{\rho}_s$ which show at most coherent dynamics:

$$\frac{d\hat{\rho}_s}{dt} \approx -\frac{i}{\hbar}[\hat{H}_0,\hat{\rho}_s] \quad \text{for } t \ll \tau_d , \tag{3.2}$$

i.e., which are not affected by fast incoherent relaxation processes. If $\hat{\rho}_s$ describes an eigenstate or a statistical mixture of eigenstates of $\hat{H}_0$, then $\hat{H}_0$ and $\hat{\rho}_s$ commute, and the quantum system I remains stationary. If, on the other hand, $\hat{\rho}_s$ describes a coherent superposition of eigenstates of $\hat{H}_0$, then $\hat{H}_0$ and $\hat{\rho}_s$ no longer commute, and the quantum system I follows periodic or quasiperiodic orbits in state space. We call these stationary states and (quasi)periodic orbits in state space the (quantum) attractors of I.

Let us denote the time scale of the fastest relaxation process by τ_r. In the regime $t \ll \tau_r$ the dynamics is coherent, and every possible state $\hat{\rho}$ is an element of an attractor manifold. For much larger times than the slowest relaxation time τ_d ($t \gg \tau_d$), on the other hand, the only attractor is the thermal equilibrium state. Nontrivial attractors therefore exist only on a time scale $\tau_r \ll t \ll \tau_d$, and critically depend on an appropriate time scale spreading ($\tau_r \ll \tau_d$) of the incoherent relaxation processes [otherwise (3.2) could not be fulfilled]. The respective basin of attraction and stability heavily leans on dissipation (cf. Ebeling[39] for classical systems). If the number of fast "dissipative," i.e., incoherent, relaxation channels is large, there exist only a few attractors, but the corresponding basins of attraction are large. As will be discussed within Sec. V B, this has consequences for the preparation process: the broader the attractor basins, the less critical is the preparation of attractors against small changes in the preparation system. The attractors of I may be characterized by the expectation values $\{n\}$ of a set of relevant observables. In what follows, we do not consider the possibility of having additional stationary states when the system is externally driven.

The open quantum system I is now coupled to an external (macroscopic) preparation system $\hat{H}_p$ and to a (macroscopic) measurement apparatus $\hat{H}_m$. The time evolution of I is then described by

$$\frac{d\hat{\rho}}{dt} = -\frac{i}{\hbar}[\hat{H}_0+\hat{H}_{0-p}+\hat{H}_{0-m},\hat{\rho}] + \left.\frac{d\hat{\rho}}{dt}\right|_{\text{incoh}} , \tag{3.3}$$

where $\hat{H}_{0-p}$ and $\hat{H}_{0-m}$ denote the coupling to the preparation and the measurement system, respectively.

We will assume that for specific ("idle") states of $\hat{H}_p$, the set of attractors $\hat{\rho}_s$ (as discussed above) is not changed. In general, however, depending on the state of $\hat{H}_p$ ("driving force") only a subset of all possible attractors remain attractors of the total system, too. Performing a switching process means driving the system from an initial attractor of I (characterized by the expectation values $\{n_i\}$) via certain transient states to a final attractor of I (characterized by the expectation values $\{n_f\}$), which is an attractor of the total system, too. The switching dynamics, as discussed in the next section, must occur on a time scale $t \ll \tau_d$, so that the decay of metastable states cannot interfere, which means that the states of $\hat{H}_p$ must change on the same time scale. After the switching process is completed, we can let the state of $\hat{H}_p$ relax to the idle state without further disturbance. This allows us to change between different attractors by means of external pulses of the states of the preparation system. Generally, for a given preparation system, not all attractors can be reached directly from every initial state within one step. But a reliable preparation of all attractors must be possible, using a limited sequence of elementary switching processes.

IV. OPTICAL CONTROL AND RELAXATION

A. Equation of motion for the reduced density matrix

We now return to the multiple heterostructure of Sec. II. It is assumed that a single hole has been trapped, i.e., that in the $T=0$ K ground state the Fermi level is pinned between level 1 and level 2. Neglecting many-particle effects, we may describe the quantum dot structure on the time scale of switching by a three-level model for a single electron:

$$\hat{H}_0 = \sum_{j=1}^{3} E_j \hat{a}_j^{\dagger} \hat{a}_j \ . \tag{4.1}$$

Here, $\hat{a}_j^{\dagger}$ and $\hat{a}_j$ are the electron creation and destruction operators. Note that spin degeneracy is lifted by spin-orbit coupling and by the spatial confinement of the quasiparticle (Coulomb interaction).[40] Possible excitations from the ground state include the transient state (electron in level 3) and the long-lived charge-transfer state as a metastable state (electron in level 2).

The preparation system couples via single modes of the electromagnetic field to the fast transitions 3-1 and 3-2 of the electronic subsystem (4.1). Since we want to investigate the preparation of coherent electronic superposition states, too, we describe the light field by phase-correlated classical plane waves with high temporal coherence:

$$\mathbf{A} = \sum_{j=1}^{2} \mathbf{A}_j \cos(\omega_j t + \phi_j) \ . \tag{4.2}$$

where we use the dipole approximation. The coupling Hamiltonian then reads

$$\hat{H}_{0-p} = 2\hbar \sum_{j=1}^{2} [\mathbf{A}_j \cos(\omega_j t + \phi_j)] \cdot \sum_{m=1}^{2} [\mathbf{G}_m \hat{a}_m^{\dagger} \hat{a}_3 + \mathbf{G}_m^{*} \hat{a}_3^{\dagger} \hat{a}_m] \ . \tag{4.3}$$

Since, on the time scale $t \ll \tau_d$, we need only to consider the photon-field reservoir, we find for the reduced density matrix[31]

$$\frac{d\hat{\rho}}{dt} = -\frac{i}{\hbar}[\hat{H}_0 + \hat{H}_{0-p}, \hat{\rho}] + \sum_{j=1}^{2} \frac{w_j}{2} ([\hat{a}_j^{\dagger} \hat{a}_3, \hat{\rho} \hat{a}_3^{\dagger} \hat{a}_j] + [\hat{a}_j^{\dagger} \hat{a}_3 \hat{\rho}, \hat{a}_3^{\dagger} \hat{a}_j]) \ , \tag{4.4}$$

where the transition probabilities w_j are given by (2.3). Using a polar representation for the complex coupling constants

$$\begin{aligned} \Omega_1 &= \mathbf{G}_1 \cdot \mathbf{A}_1 = \bar{\Omega}_1 e^{i\theta_1} \ , \\ \Omega_2 &= \mathbf{G}_2 \cdot \mathbf{A}_2 = \bar{\Omega}_2 e^{i\theta_2} \end{aligned} \tag{4.5}$$

and the off-diagonal matrix elements

$$\begin{aligned} \rho_{13} &= \bar{\rho}_{13} e^{i(\omega_1 t + \phi_1 + \theta_1)} \ , \\ \rho_{23} &= \bar{\rho}_{23} e^{i(\omega_2 t + \phi_2 + \theta_2)} \ , \\ \rho_{12} &= \bar{\rho}_{12} e^{i[(\omega_1 - \omega_2)t + (\phi_1 - \phi_2) + (\theta_1 - \theta_2)]} \ , \end{aligned} \tag{4.6}$$

we get, within a generalized rotating-wave approximation, for the transformed elements of the density matrix (in the basis of the electronic eigenstates of $\hat{H}_0$)

$$\begin{bmatrix} \dot{\rho}_{11} \\ \dot{\rho}_{22} \\ \dot{\rho}_{33} \\ \dot{\bar{I}}_{13} \\ \dot{\bar{R}}_{13} \\ \dot{\bar{I}}_{23} \\ \dot{\bar{R}}_{23} \\ \dot{\bar{I}}_{12} \\ \dot{\bar{R}}_{12} \end{bmatrix} = \begin{bmatrix} 0 & 0 & w_1 & -2\bar{\Omega}_1 & 0 & 0 & 0 & 0 & 0 \\ 0 & 0 & w_2 & 0 & 0 & -2\bar{\Omega}_2 & 0 & 0 & 0 \\ 0 & 0 & -(w_1+w_2) & 2\bar{\Omega}_1 & 0 & 2\bar{\Omega}_2 & 0 & 0 & 0 \\ \bar{\Omega}_1 & 0 & -\bar{\Omega}_1 & -\frac{1}{2}(w_1+w_2) & \delta_1 & 0 & 0 & 0 & \bar{\Omega}_2 \\ 0 & 0 & 0 & -\delta_1 & -\frac{1}{2}(w_1+w_2) & 0 & 0 & -\bar{\Omega}_2 & 0 \\ 0 & \bar{\Omega}_2 & -\bar{\Omega}_2 & 0 & 0 & -\frac{1}{2}(w_1+w_2) & \delta_2 & 0 & \bar{\Omega}_1 \\ 0 & 0 & 0 & 0 & 0 & -\delta_2 & -\frac{1}{2}(w_1+w_2) & \bar{\Omega}_1 & 0 \\ 0 & 0 & 0 & 0 & \bar{\Omega}_2 & 0 & -\bar{\Omega}_1 & 0 & \delta_1-\delta_2 \\ 0 & 0 & 0 & -\bar{\Omega}_2 & 0 & -\bar{\Omega}_1 & 0 & -(\delta_1-\delta_2) & 0 \end{bmatrix} \begin{bmatrix} \rho_{11} \\ \rho_{22} \\ \rho_{33} \\ \bar{I}_{13} \\ \bar{R}_{13} \\ \bar{I}_{23} \\ \bar{R}_{23} \\ \bar{I}_{12} \\ \bar{R}_{12} \end{bmatrix} . \tag{4.7}$$

Here, $\bar{\Omega}_1$ and $\bar{\Omega}_2$ are the respective Rabi frequencies which depend on the intensity of the incident light. δ_1 and δ_2 give the detuning of the applied light modes:

$$\hbar\delta_1 = E_3 - E_1 - \hbar\omega_1 ,$$
$$\hbar\delta_2 = E_3 - E_2 - \hbar\omega_2 . \tag{4.8}$$

ρ_{ii} denote the diagonal elements of the density matrix and $\bar{R}_{ij}$ and $\bar{I}_{ij}$ the real and imaginary parts of the transformed off-diagonal elements $\bar{\rho}_{ij}$, respectively.

B. Attractors of the three-level system

The attractors of the isolated system I (cf. Sec. III) are found from (4.7) for $\bar{\Omega}_1 = \bar{\Omega}_2 = 0$, $\delta_1 = \delta_2 = 0$, and $t \to \infty$:

$$\rho_{11}(\infty) = \rho_{11}(0) + \frac{w_1}{w_1 + w_2}\rho_{33}(0) ,$$
$$\rho_{22}(\infty) = 1 - \rho_{11}(0) ,$$
$$\bar{R}_{12}(\infty) = \bar{R}_{12}(0) , \tag{4.9}$$
$$\bar{I}_{12}(\infty) = \bar{I}_{12}(0) ,$$
$$\rho_{33}(\infty) = \bar{I}_{13}(\infty) = \bar{R}_{13}(\infty) = \bar{I}_{23}(\infty) = \bar{R}_{23}(\infty) = 0 .$$

These attractors, depending on the initial conditions, can be divided into three groups.

(1) *"Pure" attractors:* $\bar{R}_{12} = \bar{I}_{12} = 0$ *and* $\rho_{11}(0) = 1$ *or* $\rho_{11}(0) = 0$ *(pure states 1 or 2).* The quantum system remains stationary.

(2) *"Coherent" attractors: a coherent superposition of eigenstates 1 and 2.* After diagonalization the density matrix contains only one element which is not zero (zero entropy). The quantum system follows periodic orbits in state space [cf. Eq. (4.6)].

(3) *"Stochastic" attractors.* After diagonalization the density matrix contains more than one element which is not zero. Because of its finite entropy, such an attractor will induce stochastic behavior in a measurement or a further dynamical process. As long as $\bar{\rho}_{12} = 0$ the quantum system remains stationary. Otherwise it will follow a periodic orbit in state space.

These asymptotic attractors can be reached only approximately, as the time scale on which Eq. (4.4) is valid is restricted to $t \ll \tau_d$. Contrary to classical, dissipative double-well systems, which would show only a discrete set of attractors and their statistical mixture, a new class of attractors arises in their quantum-mechanical analogues: a continuous set of coherent attractors. Coherent superposition states of the eigenstates 1 and 2 do not decay for $t \ll \tau_d$, since there is no relaxation process 2-1 on this time scale.

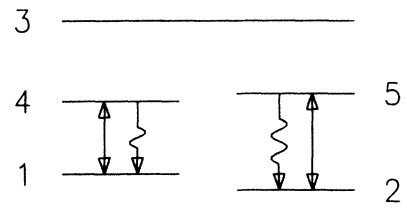

FIG. 4. Relevant subspectrum of a heterostructure for which the pure attractor states 1 and 2 can be detected via luminescence measurements. The transient levels 4 and 5 must be localized, too.

As far as the measurement of attractors is concerned, we restrict ourselves to pure attractors. During a switching process, charge is transferred from one VB well into the other and the electrical dipole moment is changed. In an experimental situation, measurement of the depolarization current could thus be performed on an ensemble of multistable elements (approximately 10^8 elementary charges). The time resolution of this technique seems to be high enough to be applied for the present purpose.

If the heterostructure has a relevant subspectrum as shown, e.g., in Fig. 4, single multistable elements may alternatively be detected via optical luminescence measurements. Measurements are performed by a test laser inducing the transitions 4-1 and/or 5-2 and detecting the spontaneously emitted photons of the corresponding energy. The number of counts may be integrated over the whole lifetime of the corresponding attractor. For attractors with long enough lifetimes the sensitivity of this method is high enough to detect single electron transitions.[41] The amplification is based on the same time-scale spreading, $\tau_r \ll \tau_d$, which is responsible for the bistable behavior.

C. Dissipative one-mode dynamics

In this section we will briefly discuss the three-level system driven by a single light mode. Without loss of generality we may assume that the light mode induces transitions between the eigenstates 1 and 3 [Fig. 5(a)]. We therefore must set $\bar{\Omega}_2 = 0$ and $\delta_2 = 0$. Equation (4.7) then decouples into two independent equations describing the time evolution of the diagonal elements and the off-diagonal elements $\bar{R}_{13}, \bar{I}_{13}$:

$$\begin{pmatrix} \dot{\rho}_{11} \\ \dot{\rho}_{33} \\ \dot{\bar{I}}_{13} \\ \dot{\bar{R}}_{13} \end{pmatrix} = \begin{pmatrix} 0 & w_1 & -2\bar{\Omega}_1 & 0 \\ 0 & -(w_1+w_2) & 2\bar{\Omega}_1 & 0 \\ \bar{\Omega}_1 & -\bar{\Omega}_1 & -\frac{1}{2}(w_1+w_2) & \delta_1 \\ 0 & 0 & -\delta_1 & -\frac{1}{2}(w_1+w_2) \end{pmatrix} \begin{pmatrix} \rho_{11} \\ \rho_{33} \\ \bar{I}_{13} \\ \bar{R}_{13} \end{pmatrix} , \tag{4.10}$$

$$\dot{\rho}_{22} = w_2\rho_{33} ,$$

and the time evolution of the other off-diagonal elements:

$$\begin{pmatrix} \dot{\bar{I}}_{23} \\ \dot{\bar{R}}_{23} \\ \dot{\bar{I}}_{12} \\ \dot{\bar{R}}_{12} \end{pmatrix} = \begin{pmatrix} -\frac{1}{2}(w_1+w_2) & 0 & 0 & \bar{\Omega}_1 \\ 0 & -\frac{1}{2}(w_1+w_2) & \bar{\Omega}_1 & 0 \\ 0 & -\bar{\Omega}_1 & 0 & \delta_1 \\ -\bar{\Omega}_1 & 0 & -\delta_1 & 0 \end{pmatrix} \begin{pmatrix} \bar{I}_{23} \\ \bar{R}_{23} \\ \bar{I}_{12} \\ \bar{R}_{12} \end{pmatrix} . \tag{4.11}$$

The only stationary state of (4.10) and (4.11) is given by the attractor $\rho_{ij}=\delta_{i2}\delta_{j2}$, independent of the choice of the parameters and independent of the initial state. Since all off-diagonal elements decay, one-mode light pulses can only be used to prepare pure attractors. Figure 6 shows the diagonal elements ρ_{11}, ρ_{22}, and ρ_{33} and the off-diagonal elements $\bar{I}_{13}$, $\bar{I}_{23}$, and $\bar{R}_{12}$ as a function of time during a switching process.

We may define a switching time T by[18,19]

$$T=\max[-(\mathrm{Re}\lambda_j)^{-1}] , \tag{4.12}$$

where λ_j are the (complex) eigenvalues of the matrix in equation (4.10). Figure 7 shows this switching time T for different detuning and Rabi frequencies. For high values of $\bar{\Omega}_1/(w_1+w_2)$ the switching time is limited by the spontaneous emission $3\rightarrow 2$ and attains a minimal value $T=2/w_2$ independent of the detuning (cf. Ref. 18 for the case $w_1=0$). This may lead to problems with the selective preparation of individual three-level systems within an array of several quantum dots. Let us consider two three-level systems with transition frequencies separated by $\delta_1=10(w_1+w_2)$. Using light with low intensity $[\bar{\Omega}_1=0.2(w_1+w_2)]$, both systems may be switched selectively since the ratio of the corresponding switching times is 10^3. Irradiation with light of high intensity $[\bar{\Omega}_1=10(w_1+w_2)]$, on the other hand, leads to switching times which are nearly identical, so that selective switching is no longer possible (cf. also Sec. V B).

D. Dissipative two-mode dynamics

The three-level system is now driven by two different light modes, which induce transitions between the eigenstates 3-1 and 3-2, respectively [Fig. 5(b)]. The system must be described by the full set of equations (4.7). Figure 8 shows the stationary population of level 3 for different detuning asymmetry $\Delta=\delta_1-\delta_2$. If the two light modes are asymmetrically detuned ($\Delta\neq 0$), the population of level 3 is not zero and the attractor of the total

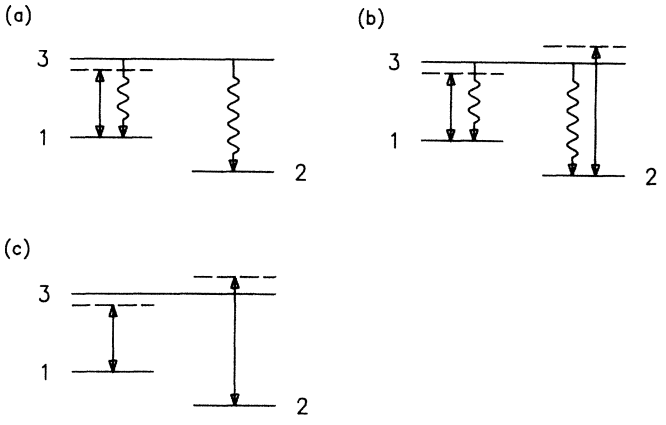

FIG. 5. Quantum optical models for the interaction of a multistationary three-level system with single modes of the electromagnetic field as discussed in the text. (a) dissipative one-mode dynamics, (b) dissipative two-mode dynamics, (c) coherent two-mode dynamics.

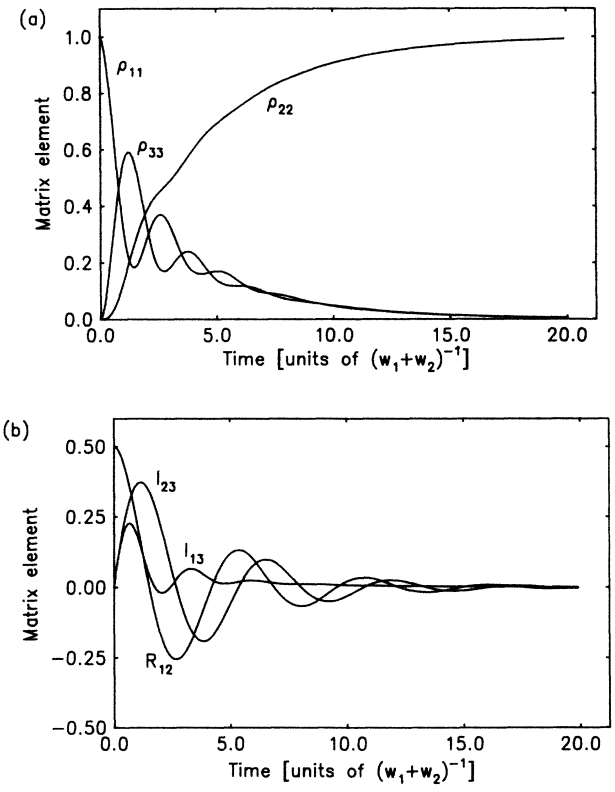

FIG. 6. Matrix elements of the density matrix as a function of time for a dissipative one-mode process. Parameters: $\bar{\Omega}_1=1.2(w_1+w_2)$, $\delta_1=0$, $w_1=w_2$. (a) Diagonal elements as a function of time for a pure initial state: $\rho_{ij}(0)=\delta_{i1}\delta_{j1}$. (b) Off-diagonal elements as a function of time for a coherent initial state: $\rho_{11}(0)=\rho_{22}(0)=0.5$, $\bar{R}_{12}(0)=0.5$.

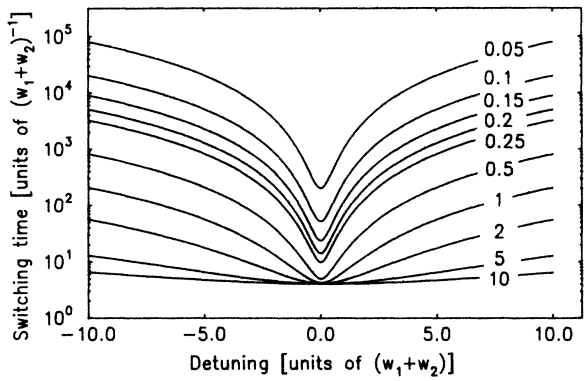

FIG. 7. Switching time T of a dissipative one-mode process for different detuning and Rabi frequencies. The figure shows T for $\bar{\Omega}_1=0.05$, 0.1, 0.15, 0.2, 0.25, 0.5, 1, 2, 5, and 10 in units of (w_1+w_2) and for $w_1=w_2$.

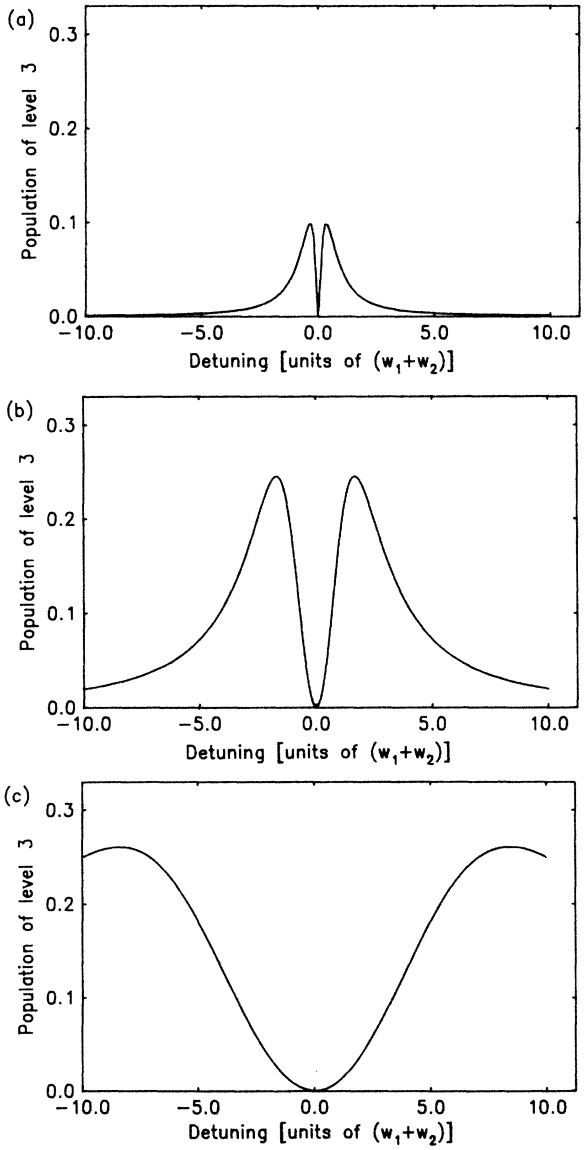

FIG. 8. Stationary population of level 3 for different detuning asymmetries Δ and different Rabi frequencies. Parameters: $\delta_1=0$, $w_1=w_2$. (a) $\bar{\Omega}_1=\bar{\Omega}_2=0.2(w_1+w_2)$, (b) $\bar{\Omega}_1=\bar{\Omega}_2=(w_1+w_2)$, (c) $\bar{\Omega}_1=\bar{\Omega}_2=5(w_1+w_2)$.

system is no longer an attractor of the isolated quantum system I (cf. Sec. III). A complete switching process therefore consists of a light pulse of finite duration, followed by a relaxation process ($\bar{\Omega}_1=\bar{\Omega}_2=0$), which drives the system into a stochastic attractor. If the two light modes are symmetrically detuned ($\Delta=0$), the population of level 3 tends to zero for long enough light pulses and the population is coherently trapped within the electronic states 1 and 2. This effect is known as coherent population trapping and is found only if the driving light modes are correlated.[42] The stationary state is given by

$$\rho_{11}=\frac{\bar{\Omega}_2^2}{\bar{\Omega}_1^2+\bar{\Omega}_2^2},\quad \rho_{22}=\frac{\bar{\Omega}_1^2}{\bar{\Omega}_1^2+\bar{\Omega}_2^2},\quad R_{12}=-\frac{\bar{\Omega}_1\bar{\Omega}_2}{\bar{\Omega}_1^2+\bar{\Omega}_2^2} \tag{4.13}$$

while all other matrix elements are zero. Dissipative two-mode dynamics may therefore be used to prepare coherent attractors; the actual attractor is selected by an appropriate choice of the Rabi frequencies, i.e., by an appropriate choice of the intensity of the incident light. The preparation of the coherent attractor is independent of the detuning (as long as $\Delta=0$), the spontaneous emission rates, and the initial state, but critically dependent on the detuning asymmetry. The smaller the Rabi frequencies $\bar{\Omega}_1$ and $\bar{\Omega}_2$, the more sensitive the preparation will be to small values of Δ (Fig. 8). Figure 9 shows the time dependence of the diagonal and some of the off-diagonal elements of the density matrix during a preparation process.

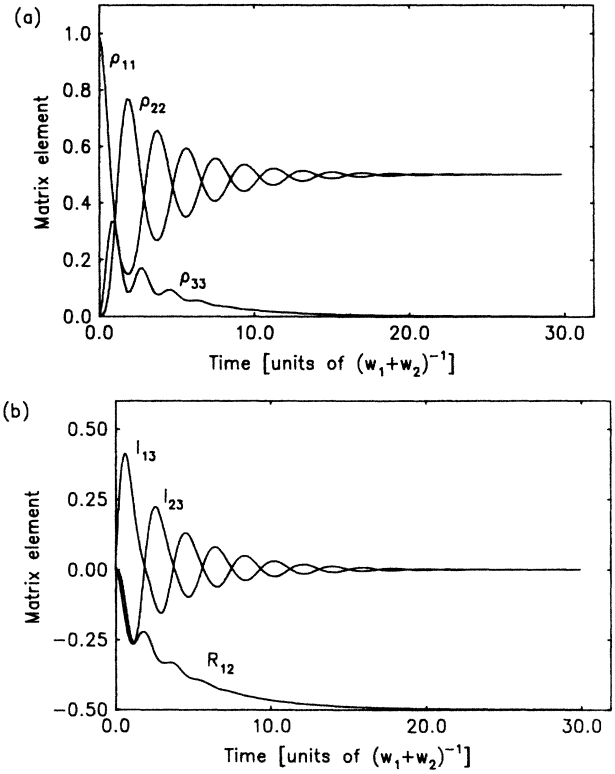

FIG. 9. Matrix elements of the density matrix as a function of time for a dissipative two-mode process. Parameters: $\bar{\Omega}_1=\bar{\Omega}_2=1.2(w_1+w_2)$, $\delta_1=\delta_2=0$, $w_1=w_2$, and $\rho_{ij}(0)=\delta_{i1}\delta_{j1}$. (a) Diagonal elements, (b) off-diagonal elements.

E. Coherent two-mode dynamics

If the time scale of the switching dynamics becomes much shorter than the time scale of the spontaneous emission, also the coupling to the external photon vacuum may be neglected: $w_1=w_2=0$. The three-level system will undergo coherent transitions between the eigenstates 3-1 and 3-2, [Fig. 5(c)]. For $w_1=w_2=0$ Eq. (4.7) can be reduced to three coupled second-order differential equations for the off-diagonal elements $\bar{I}_{ij}$:

$$\begin{bmatrix} \ddot{\bar{I}}_{13} \\ \ddot{\bar{I}}_{23} \\ \ddot{\bar{I}}_{12} \end{bmatrix} = \begin{bmatrix} -(\delta_1^2+4\bar{\Omega}_1^2+\bar{\Omega}_2^2) & -3\bar{\Omega}_1\bar{\Omega}_2 & -\bar{\Omega}_2(2\delta_1-\delta_2) \\ -3\bar{\Omega}_1\bar{\Omega}_2 & -(\delta_2^2+4\bar{\Omega}_2^2+\bar{\Omega}_1^2) & -\bar{\Omega}_2(2\delta_2-\delta_1) \\ -\bar{\Omega}_2(2\delta_1-\delta_2) & -\bar{\Omega}_2(2\delta_2-\delta_1) & -[\bar{\Omega}_1^2+\bar{\Omega}_2^2+(\delta_1-\delta_2)^2] \end{bmatrix} \begin{bmatrix} \bar{I}_{13} \\ \bar{I}_{23} \\ \bar{I}_{12} \end{bmatrix} \tag{4.14}$$

which can be solved analytically for symmetrical detuning ($\delta_1=\delta_2=\delta$). For the diagonal elements of the density matrix we obtain a superposition of oscillations with frequencies[18,43]

$$\lambda=2(\bar{\Omega}_1^2+\bar{\Omega}_2^2+\tfrac{1}{4}\delta^2)^{1/2} \quad \text{and} \quad \lambda_\pm=\tfrac{1}{2}(\lambda\pm\delta)\ . \tag{4.15}$$

As has been shown in Ref. 18, with $\bar{\Omega}_1=\bar{\Omega}_2$ and $\delta_1=\delta_2$ it is possible to transfer an electron coherently from level 1 to level 2 with probability 1. The off-diagonal elements vanish just when the diagonal elements are in their extremum. Coherent two-mode processes may therefore be used to prepare pure attractors, too. We define the required pulse length T as the time for complete electron transfer. We get $T=\pi(\bar{\Omega}_1^2+\bar{\Omega}_2^2)^{-1/2}$ which, in principle, can be made much shorter than in the case of the dissipative dynamics. However, high laser powers are needed to obtain short enough switching times (e.g., $P\approx 3\times 10^3$ W/m^2 for $T=1$ ps and the heterostructure of Table I, $\beta=1.5$). Furthermore, the preparation process is now sensitive to the Rabi frequencies,[18] finite detuning δ (Fig. 10), and the light-pulse length. The final state depends on the initial state, too, as shown in Fig. 11: during a light pulse with duration T the populations of level 1 and level 2 get interchanged.

V. INFORMATION PROCESSING BY INDIVIDUAL MULTISTABLE ELEMENTS

A. Preliminaries

Although the model structure discussed is a microscopic system whose dynamics must be described within the framework of quantum mechanics, multistationarity and complex dynamics is achieved in a quite conventional way: complex selection rules arise due to a separation of the microscopic degrees of freedom into dynamical and passive degrees of freedom on the time scale of the switching process. This has been demonstrated for the case of the electron-phonon interaction. We believe that a hierarchical structure of the degrees of freedom is a necessary condition for every information processing system. The character of the stationary states, on the other hand, is novel: Contrary to optical computers or conventional microprocessors, the stationary states are metastable states of the isolated computing system and do not require an external driving apparatus (e.g., a battery). Therefore no dissipation of energy is needed to maintain the stationary state; dissipation of energy is only required during the switching process (cf. Sec. IV). This may be an advantage in the construction of highly packed devices, where the dissipated energy is a severe problem.

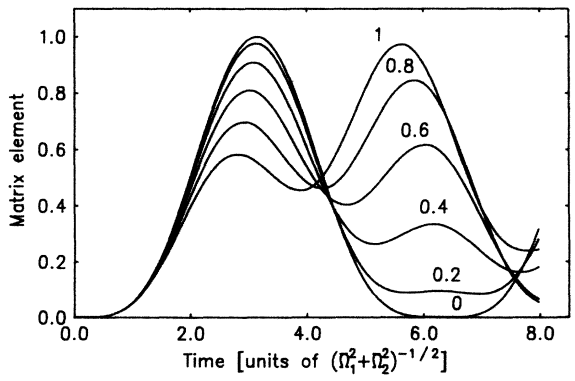

FIG. 10. Population of level 2 as a function of time and detuning. Parameters: $\bar{\Omega}_1=\bar{\Omega}_2$, $\delta_1=\delta_2=0$, 0.2, 0.4, 0.6, 0.8, 1 in units of $(\bar{\Omega}_1^2+\bar{\Omega}_2^2)^{1/2}$, and $\rho_{ij}(0)=\delta_{i1}\delta_{j1}$. Finite detuning destroys the switching process.

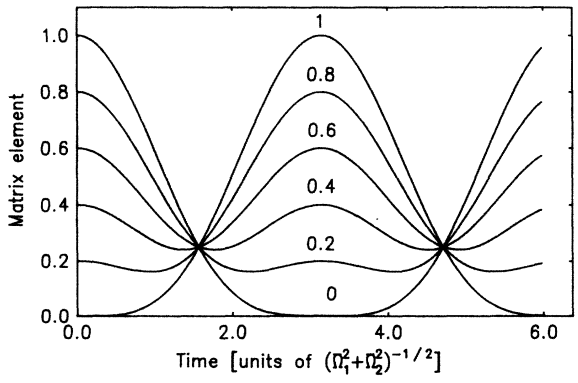

FIG. 11. Population of level 2 as a function of the initial state. Parameters: $\bar{\Omega}_1=\bar{\Omega}_2$, $\delta_1=\delta_2=0$, $\rho_{11}(0)=1-\rho_{22}(0)=0$, 0.2, 0.4, 0.6, 0.8, 1, and all other matrix elements zero (stochastic initial state).

Three-level systems are the most elementary bistable systems which can store information on a time scale $t \ll \tau_d$. If we restrict ourselves to the pure attractors, each three-level system can store one bit. There are two switching processes possible which can be used to prepare those attractors: "dissipative" one-mode light pulses and "coherent" two-mode light pulses. Since the final state of the three-level system does not depend on the initial state, dissipative one-mode switching is capable of overwriting single bits. Both switching processes differ in their susceptibility for errors and in the role of dissipation in the switching process.

By assigning an alphabet to at least some of the attractors, we can use the open quantum system to store and process information ("quantum computer"). To do so, a reliable preparation of the attractors representing information must be possible within a finite sequence of relaxation processes. Likewise, the measuring process must reliably reveal the information encoded in the final attractor on a time scale much smaller than the dwell time τ_d. The probability that identical measurements, performed on two identical quantum systems in different attractors $\hat{\rho}_i$ and $\hat{\rho}_j$, yield the same result, must be negligibly small for at least one of the relevant observables (denoted with $\hat{M}$)

$$|\,\mathrm{tr}(\hat{\rho}_i\hat{M}^2)-[\mathrm{tr}(\hat{\rho}_i\hat{M})]^2\,|^{1/2} \ll |\,\mathrm{tr}(\hat{\rho}_i\hat{M})-\mathrm{tr}(\hat{\rho}_j\hat{M})\,| \quad \text{for all } i\neq j \qquad (5.1)$$

For a given measurement system condition (5.1) restricts the number of attractors of the system capable of representing information.

B. Information storage: Errors and role of dissipation

Errors occurring during a switching process can be separated into two classes: errors due to a "wrong" Hamiltonian $\hat{H}_0$ (type-1 errors) and errors due to a wrong coupling Hamiltonian $\hat{H}_{0-p}$ (type-2 errors). Type-1 errors may arise from nonideal interfaces, fabrication failures, and failure of the idealized description due to, e.g., many-body effects and heavy-hole–light-hole mixing. Errors of this kind change the electronic elementary excitations and alter the time scale of the relaxation processes. As long as the errors are small, so that the time scale of the stability of the attractors and the time scale of the switching dynamics are still well separated, type-1 errors have no serious effect.

Type-2 errors may arise from, e.g., off-resonance light modes, wrong light-pulse length, and wrong light intensity. They directly influence the switching process. In the case of dissipative switching, only one (asymptotic) stationary state exists, which is therefore independent of the light-pulse parameters. For wrong light-pulse parameters reliable switching is still possible, but the switching time T increases (cf. Fig. 7). For a single element, errors can be made arbitrarily small by using sufficiently long pulses, provided $t \ll \tau_d$ is still fulfilled and the transition frequency for the back-transfer is far off resonance.

If several bistable elements are combined to a quantum information memory, another kind of error arises. Due to the finite linewidth of the optical transitions, a bistable element may be switched even if the light mode is off resonance. This leads to a finite bandwidth per transition and a maximal density of the transitions in frequency space, which depends on the intensity of the incident light and the tolerable error probability. Let us imagine two three-level systems with slightly different transition frequencies, one of them (I) should be switched selectively. The total error probability consists of the probability w_{I} that system I has not been switched during the pulse duration T, and the probability w_{II} that the other system (II), despite being off resonance, has been switched within this time. Figure 12 shows the total error probability $w_e = w_{\mathrm{I}} + w_{\mathrm{II}}$ as a function of the pulse duration T. For a short pulse-length T the total error probability is large, since the switching process of system I has a finite switching time. The probability w_e then decreases until the pulse length becomes comparable with the switching time of the off-resonance system II. Contrary to a single three-level system, the error probability cannot be made arbitrarily small within an array of elementary storage elements. There exists an optimal pulse length for which the error probability is minimal; its magnitude depends on the light intensity, as well as the separation δ in frequency space. If we choose an optimal Rabi frequency $\bar{\Omega}_1 = 0.5(w_1 + w_2)$ and accept one wrong switching process out of $\approx 6\times 10^4$, the minimal separation of storage elements in frequency space will be approximately 10^{10} Hz [i.e., $\delta = 100(w_1 + w_2)$, cf. Fig. 12]. Since the useful transition frequencies for a typical semiconductor material (e.g., in the $Ga_{1-x}Al_xAs$ system) lie within a range of approximately 1.6×10^{13} Hz, 1600 different elements could be selectively switched. A high number of storage elements may be achieved by spatially resolved addressing of the three-level systems. If we assume that the diameter of a focused laser spot is about 10 μm (Ref. 17), we can derive a maximal information density of about 10^9 bits/cm^2. An error of rate 10^{-4}–10^{-3} is, of course, quite large, so that redundancy must be used.

Coherent switching processes lead to an accumulation of errors within each step. Integrating (4.14), we get for

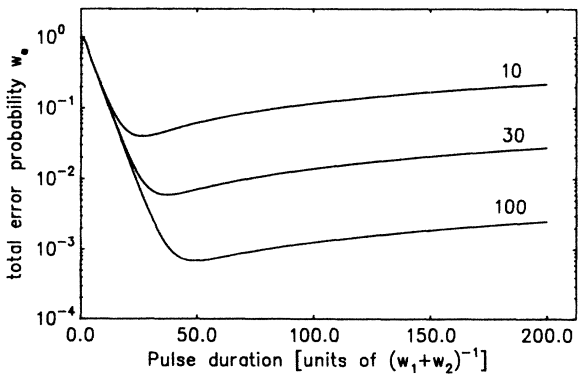

FIG. 12. Total error probability w_e as a function of the pulse duration. The light-pulse parameters are $\bar{\Omega}_1 = 0.5(w_1 + w_2)$, $w_1 = w_2$ for both elements I and II. The transition frequency is resonant for system I, but system II is detuned by $\delta = 10$, 30, or 100 in units of $(w_1 + w_2)$.

the population of level 2 with the initial condition $\rho_{ij}(0)=\delta_{i1}\delta_{j1}$

$$\rho_{22}(t)=\overline{\Omega}_1^2\overline{\Omega}_2^2\left[2\frac{\cos(\lambda t)-1}{\lambda^2}-\frac{\cos(\lambda_+ t)-1}{\lambda_+^2}-\frac{\cos(\lambda_- t)-1}{\lambda_-^2}\right]. \tag{5.2}$$

The correct parameter combination for a switching process is given by $\overline{\Omega}_1=\overline{\Omega}_2$, $\delta=0$, and pulse duration $T=\pi(\overline{\Omega}_1^2+\overline{\Omega}_2^2)^{-1/2}$. There are three kinds of type-2 errors possible.

(1) *Wrong Rabi frequencies* ($\overline{\Omega}_1\neq\overline{\Omega}_2$). For the error probability we get

$$\Delta\rho_{22}=1-\rho_{22}(T)=\left[\frac{1-\overline{\Omega}_2/\overline{\Omega}_1}{1+\overline{\Omega}_2/\overline{\Omega}_1}\right]^2. \tag{5.3}$$

(2) *Finite detuning* ($\delta\neq 0$). In the lowest order of δ we get for the error probability

$$\Delta\rho_{22}=1-\rho_{22}(T)=\frac{1}{4}\left[\frac{\pi^2}{16}+1\right]\frac{\delta^2}{\overline{\Omega}_1^2+\overline{\Omega}_2^2}. \tag{5.4}$$

(3) *Wrong pulse duration* ($\tau=T+\Delta\tau$). In lowest order of $\Delta\tau$ we get for the error probability

$$\Delta\rho_{22}=1-\rho_{22}(\tau)=\tfrac{1}{2}\Delta\tau^2(\overline{\Omega}_1^2+\overline{\Omega}_2^2). \tag{5.5}$$

Errors in the initial preparation are not changed during a switching process (cf. Fig. 11). Since the final state depends on the initial condition, overwriting of single bits is no longer possible. Coherent switching is therefore not practical for simple storage elements, but may be useful in performing simple logical operations, as shown in the next chapter.

Dissipation of energy by coupling to external reservoirs leads to transitions between the electronic eigenstates of the open quantum system. Dissipation is not only a possible source of errors (type-1 errors), but it is a necessary element to make the switching process less susceptible to type-2 errors. Within our model, dissipation has to fulfill several tasks. The coupling to appropriate reservoirs is needed (1) to prepare an attractor independent of the initial attractor of the quantum system, (2) to fix the result of a switching step, and (3) to make the switching process less susceptible to type-2 errors.

In the case of dissipative one-mode processes all tasks are performed by the coupling of $\hat{H}_0$ to the spontaneous emission modes of the electromagnetic field. Independent of the changes in $\hat{H}_{0-p}$, i.e., in the light-pulse parameters $\overline{\Omega}_1$ and δ_1, only one attractor of the system I remains attractor of the total system, too (cf. Sec. III). In the case of coherent two-mode pulses no dissipation occurs within $\hat{H}_0$. Therefore the system is susceptible to type-2 errors and no longer capable of performing task 1. It is remarkable that fixing of the result still occurs, without dissipating energy within the computing system, but in the remote system $\hat{H}_p$ responsible for the laser pulse.

To perform tasks 1–3, we exploit two different properties of a reservoir: We make use of the fact that a reservoir consists of "irrelevant" degrees of freedom (task 1) and that the number of its degrees of freedom is large (tasks 2 and 3). Since the performance of task 1 does not rely on the number of irrelevant degrees of freedom, coupling to a reservoir is not a universal prerequisite, although we use it in our model. If one relies on just a few irrelevant degrees of freedom, relevant and irrelevant degrees of freedom may be treated physically on equal footing: The distinction between them will be made by assigning an appropriate alphabet to the attractors. Attractors which differ only in the projection onto the irrelevant subspace have the same meaning. This concept, e.g., has been used for the (theoretical) construction of a reversible computer.[24,26,28] The performance of tasks 2 and 3, on the other hand, depends on a large reservoir. For a reliable fixation of the result, the Poincare recursion time must be at least of the order of the dwell time τ_d. This is accomplished in our model by assuming a totally absorbing reservoir which, by definition, has an infinite recursion time. Task 3 relies on large basins of attraction in the relevant subspace which, in turn, exist only for a large number of irrelevant degrees of freedom.

C. Logical functions with one argument

While the final state generally depends on the initial state in the case of coherent light pulses, the same is true for dissipative dynamics only if the multistable system under consideration has more than two pure attractors (Fig. 13). If the switching electron is initially in the attractor state 5, a dissipative process induced by a light pulse with frequency ω_{45} will transport the electron into the attractor state 3, while an electron in state 1 will be unaffected. These dynamics may be used to represent logical functions with one argument. Logical functions with two arguments as well as concepts for the general purpose computer make use of several interacting electrons and are discussed in the following paper.[14] We first relate the attractors to an alphabet for which we may choose the binary digits. In the following, two out of the

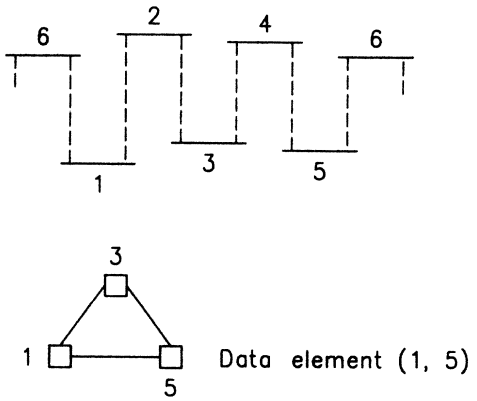

FIG. 13. Cyclic quantum optical model and coupling scheme of the pure attractors for a multistable element capable of performing logical functions. The system consists of three pure attractors (1, 3, and 5), the highest VB states, and three transient states (2, 4, and 6), the lowest CB states.

three (stationary) attractor states in Fig. 13 are taken to represent one bit of information: electron in 5, logical state 0; electron in 1, logical state 1; electron in 3, logical state is not defined. There are four logical functions with one argument:

Argument	0	Identity	NOT	1
0	0	0	1	1
1	0	1	0	1

The functions 0 and 1 are nothing else but WRITE operations which store data into a bistable storage element, consisting of the energy levels 1, 6, and 5. They have been discussed within the last chapter. For a realization of the NOT operation, three consecutive dissipative switching processes (single light modes) are necessary:

$$\begin{array}{cccccccc} 0 & \{5\} & & \{3\} & & \{3\} & & \{1\} \quad 1 \\ & & \rightarrow\omega_{45}\rightarrow & & \rightarrow\omega_{61}\rightarrow & & \rightarrow\omega_{23}\rightarrow & \\ 1 & \{1\} & & \{1\} & & \{5\} & & \{5\} \quad 0 \end{array}$$

Since the NOT operation is the only operation (besides the trivial identity), where the final state depends on the initial state, it is the only operation which may be performed also using coherent dynamics, realized, e.g., by a coherent two-mode pulse within the three-level system 1, 6, and 5.

VI. SUMMARY

In this paper we have shown that it may be possible to construct multistationary quantum systems on the basis of semiconductor heterostructures. Although a semiconductor is a typical many-body system, it should be possible to generate quasimolecular subsystems of only a few electrons which decouple from the rest on an appropriate time-scale. As will be shown in the second part, these molecular subsystems, if properly designed, can perform the essential logical operations and may therefore be used to construct even a universal computer whose dynamical behavior must be described within the framework of quantum mechanics. The dynamics necessary to support logical operations is achieved using a separation of length, time, and energy scales, which, in turn, are based on the hierarchical nature of various degrees of freedom.

Preparation and optical control of the switching processes are performed by driving the open quantum system via single modes of the electromagnetic field. All three types of attractors may be prepared optically. Measurements may be performed optically, as well as by the determination of depolarization currents.

Arrays of three-level systems, e.g., in a semiconductor heterostructure, may be used to design an optical mass memory based on PHB (persistent hole burning) processes[17] and using dissipative switching processes between pure attractors. In PHB elements in a semiconductor heterostructure, data may be read and written on the time scale of the switching process. If properly designed, reading and writing processes can be decoupled.

Two-dimensional semiconductor heterostructures with a layer thickness of a few nanometers can presently be manufactured with high precision. Since "optical switching" and the separation of time scales mainly depends on the localization behavior of the envelope wave function in one dimension, layered structures will show optical switching and bistability, too, and might be used to establish an upper bound for the well-1 to well-2 relaxation rates from existing structuring technologies.

ACKNOWLEDGMENTS

We would like to thank Professor Hermann Haken for valuable discussions. Financial support by the Deutsche Forschungsgemeinschaft (SFB 329, Physikalische und chemische Grundlagen der Molekularelektronik) is gratefully acknowledged.

APPENDIX A

In this Appendix we outline the calculation of spectrum and eigenfunctions for the heterostructure shown in Fig. 1. For the interfaces perpendicular to the z axis we take the usual matching conditions:[44]

$$\begin{aligned} &\psi^i_{n\mathbf{k}} \mid_{\text{interface}} = \psi^j_{n\mathbf{k}} \mid_{\text{interface}} , \\ &\frac{1}{m^*_{ni}} \frac{\partial}{\partial z} \psi^i_{n\mathbf{k}} \Big|_{\text{interface}} = \frac{1}{m^*_{nj}} \frac{\partial}{\partial z} \psi^B_{n\mathbf{k}} \Big|_{\text{interface}} , \end{aligned} \tag{A1}$$

where $(i,j)=(A,B)$ or (B,C) and n denotes the CB or VB. To simplify the numerical calculations we describe the interface along the coating material by an infinite barrier, which imposes the boundary condition

$$\psi_{n\mathbf{k}} \mid_{\text{boundary}} \equiv 0 \tag{A2}$$

on the envelope function. With the ansatz

$$\psi_{n\mathbf{k}}(\mathbf{r}) = \xi_{nk_x}(x)\xi_{nk_y}(y)\chi_{n\kappa}(z) , \tag{A3}$$

Eqs. (4.2), (A1), and (A2) decouple into three one-dimensional eigenvalue problems if the potential $U(\mathbf{r})$ is additive.

In the following we take $U(\mathbf{r})=0$, i.e., we assume no external fields. We get then

$$\begin{aligned} &\xi_{nk_x}(x) = \left[\frac{2}{S}\right]^{1/2} \sin(k_x x), \quad k_x = \frac{\pi n_x}{S} \\ &\xi_{nk_y}(y) = \left[\frac{2}{S}\right]^{1/2} \sin(k_y y), \quad k_y = \frac{\pi n_y}{S}, \quad n_x, n_y \in N \\ &E^i_n(k_x,k_y) = \frac{\hbar^2(k_x^2+k_y^2)}{2m^*_{ni}} , \end{aligned} \tag{A4}$$

and

$$\begin{aligned} &-\frac{\hbar^2}{2m^*_{ni}} \frac{d^2}{dz^2} \chi^i_{n\kappa}(z) = [E_{n\kappa} - E^i_n(k_x,k_y) - E^i_n]\chi^i_{n\kappa}(z) , \\ &\chi^i_{n\kappa} \mid_{\text{interface}} = \chi^j_{n\kappa} \mid_{\text{interface}} , \\ &\frac{1}{m^*_{ni}} \frac{d}{dz} \chi^i_{n\kappa} \Big|_{\text{interface}} = \frac{1}{m^*_{nj}} \frac{d}{dz} \chi^j_{n\kappa} \Big|_{\text{interface}} , \\ &\chi^A_{n\kappa}(0) = \chi^C_{n\kappa}(L) = 0 , \end{aligned} \tag{A5}$$

where L denotes the length of the three-block structure in the z direction and S is its length in the x and y directions. The envelope functions $\chi_{n\kappa}(z)$ have the form

$$\chi_{n\kappa}(z)=A^i_{n\kappa}\cos[k^i_{n\kappa}(z-d_i)]+B^i_{n\kappa}\sin[k^i_{n\kappa}(z-d_i)]\ ,$$
$$k^i_{n\kappa}=\left[\frac{2m^*_{ni}}{\hbar^2}[E_{n\kappa}-E^i_n(k_x,k_y)-E^i_n]\right]^{1/2}\ , \qquad i=A,B,C\ . \tag{A6}$$

Here z is taken within the material $i=A$, B, and C. The coefficients $A^i_{n\kappa}$ and $B^i_{n\kappa}$ and the eigenenergy $E_{n\kappa}$ must be computed numerically.

The effective-mass theory as formulated in Eqs. (2.2) and (A1)–(A6) is valid for nondegenerate bands, i.e., for the conduction band of most of the technologically important semiconductors. Degenerate bands, i.e., the valence bands of most of the semiconductors, must generally be treated within a Kane-type model.[45] Fortunately the heavy-hole band in all semiconductors with cubic or zinc-blende symmetry completely decouples from the neighboring bands in the case $k_x=k_y=0$ (Ref. 46) and can be treated for small k_x and k_y within a parabolic approximation.

APPENDIX B

For the calculation of the interband relaxation rates, we insert the wave function (2.1) into the matrix element (2.4). Using the dipole approximation we get

$$\begin{aligned}M^{\rm opt}_{n\mathbf{k},n'\mathbf{k}',q\nu}=b^2\sum_j e^{i\mathbf{q}\cdot\mathbf{r}_j}[\psi^*_{n\mathbf{k}}(\mathbf{r}_j)\mathbf{e}_{q\nu}\cdot\nabla\psi_{n'\mathbf{k}'}(\mathbf{r}_j)]\\ \times\int_{\text{unit cell}j}u^*_{n0}u_{n'0}d^3r\\ +b^2\sum_j e^{i\mathbf{q}\cdot\mathbf{r}_j}[\psi^*_{n\mathbf{k}}(\mathbf{r}_j)\psi_{n'\mathbf{k}'}(\mathbf{r}_j)]\\ \times\int_{\text{unit cell}j}u^*_{n0}\mathbf{e}_{q\nu}\cdot\nabla u_{n'0}d^3r\ ,\end{aligned} \tag{B1}$$

where we have made use of the fact that the envelope function is slowly varying and may be approximately set constant over a unit cell. The first term in (B1) vanishes because of the orthogonality of the Bloch functions. If we replace the summation over all unit cells j by an integration, Eq. (2.3) together with (B1), (A3), and (A4) gives the result

$$w^{\rm opt}_{n\mathbf{k},n'\mathbf{k}'}=\frac{\hbar e^2\omega}{2\pi\epsilon_0 m^2c^3}\overline{(\Pi^{\rm opt}_{nn'})^2}\delta_{k_x,k'_x}\delta_{k_y,k'_y}\left|\int\chi^*_{n\kappa}\chi_{n'\kappa'}dz\right|^2\ , \tag{B2}$$

where

$$\overline{(\Pi^{\rm opt}_{nn'})^2}=\frac{1}{8\pi}\sum_{\nu=1}^{2}\int\left|\int_{\text{unit cell}}u^*_{n0}\mathbf{e}_{q\nu}\cdot\nabla u_{n'0}d^3r\right|^2d\Omega \tag{B3}$$

denotes the average Bloch matrix element in the dipole approximation. It has been taken equal for the different materials in the heterostructure. Equation B2 shows that the interband relaxation rate is directly proportional to the overlap integral:

$$w^{\rm opt}_{n\mathbf{k},n'\mathbf{k}'}\propto\left|\int\chi^*_{n\kappa}\chi_{n'\kappa'}dz\right|^2\ . \tag{B4}$$

APPENDIX C

For the calculation of the interwell relaxation rate, we insert the wave function (2.1) into the phonon matrix element (2.7):

$$M^{\rm ph}_{n\mathbf{k},n\mathbf{k}',\mathbf{q}}=b^2\Pi^{\rm ph}_{n\mathbf{q}}\sum_j\psi^*_{n\mathbf{k}}(\mathbf{r}_j)e^{i\mathbf{q}\cdot\mathbf{r}_j}\psi_{n\mathbf{k}'}(\mathbf{r}_j)\ , \tag{C1}$$

$$\Pi^{\rm ph}_{n\mathbf{q}}=\int_{\text{unit cell}j}u^*_{n0}e^{i\mathbf{q}\cdot(\mathbf{r}-\mathbf{r}_j)}u_{n0}d^3r\ . \tag{C2}$$

Again we have made use of the fact, that the envelope function is slowly varying and may be set approximately constant over a unit cell. Inserting (C1) together with (A3) and (A4) into Eq. (2.6) gives the result

$$\begin{aligned}w^{\rm ph}_{n\mathbf{k},n\mathbf{k}'}=\frac{D_1^2}{8\pi^2\rho v}\int_{\rm BZ}q[n(\mathbf{q})+\tfrac{1}{2}\mp\tfrac{1}{2}]\,|\,\Pi^{\rm ph}_{n\mathbf{q}}\,|^2\\ \times|\,\tilde{M}^{\rm ph}_{n\mathbf{k},n\mathbf{k}',\mathbf{q}}\,|^2\\ \times\delta(E_{n\mathbf{k}}-E_{n\mathbf{k}'}\pm\hbar vq)d^3q\ ,\end{aligned} \tag{C3}$$

where

$$\begin{aligned}\tilde{M}^{\rm ph}_{n\mathbf{k},n\mathbf{k}',\mathbf{q}}=\frac{4}{S^2}\left[\int_0^S\sin(k_xx)e^{iq_xx}\sin(k'_xx)dx\right]\\ \times\left[\int_0^S\sin(k_yy)e^{iq_yy}\sin(k'_yy)dy\right]\\ \times\left[\int_0^L\chi^*_{n\kappa}(z)e^{iq_zz}\chi_{n\kappa}(z)dz\right]\ .\end{aligned} \tag{C4}$$

For the Bloch matrix element we get

$$0<|\,\Pi^{\rm ph}_{n\mathbf{q}}\,|^2\le 1\ . \tag{C5}$$

In order to get an estimate of the time scales, we use the upper bound $|\,\Pi^{\rm ph}_{n\mathbf{q}}\,|^2=1$. One integration in (C3) may be readily evaluated if the BZ is approximated by a sphere with radius $q_{\max}=\pi/a$, where a is the lattice constant. In spherical coordinates we find

$$\begin{aligned}w^{\rm ph}_{n\mathbf{k},n\mathbf{k}'}=\frac{2D_1^2}{\pi^2\rho\hbar v^2S^4}\sum_{\mathbf{k}'}q^3[n(q)+\tfrac{1}{2}\mp\tfrac{1}{2}]\int_{-\pi/2}^{\pi/2}\sin\theta\,|\,I_{z\kappa\kappa'}(q\cos\theta)\,|^2\\ \times\int_0^{2\pi}|\,I_{xk_xk'_x}(q\sin\theta\cos\phi)\,|^2\,|\,I_{yk_yk'_y}\,|\,(q\sin\theta\sin\phi)\,|^2d\phi\,d\theta\ ,\end{aligned} \tag{C6}$$

$$q=\frac{1}{\hbar v}\,|E_{n\mathbf{k}}-E_{n\mathbf{k}'}|\le q_{\max}\ ,$$

where $I_{z\kappa\kappa'}$, $I_{xk_xk_x'}$, and $I_{yk_yk_y'}$ denote the three integrals in Eq. (C4). Using (A6), analytical expressions can be given for each integral. For a discussion see, e.g., Ref. 47. The two remaining integrals in (C6) have to be evaluated numerically.

An upper bound of the squared matrix elements (C4) may be found using

$$\left|\int \chi^*_{n\kappa}e^{iq_zz}\chi_{n\kappa'}dz\right|^2\le\left[\int|\chi_{n\kappa}|\,|\chi_{n\kappa'}|\,dz\right]^2. \tag{C7}$$

Within this approximation we get for the transition probability (C3)

$$w^{\rm ph}_{n\mathbf{k},n\mathbf{k}'}\propto\left[\int|\chi^*_{n\kappa}|\,|\chi_{n\kappa'}|\,dz\right]^2. \tag{C8}$$

[1]R. P. Feynman, Opt. News **11**, 11 (1985).

[2]*Molecular Electronic Devices,* edited by F. L. Carter (Marcel Dekker, New York, 1982).

[3]J. M. Lehn, Science **227**, 849 (1985).

[4]R. C. Haddon and A. A. Lamola, Proc. Natl. Acad. Sci. **82**, 1874 (1985).

[5]M. Sugi, J. Mol. Electron. **1**, 3 (1985).

[6]S. Roth, Z. Phys. **B64**, 25 (1986).

[7]F. L. Carter, in *Molecular Elecronic Devices,* Ref. 2, p. 51.

[8]F. L. Carter, Physica D **10**, 175 (1984).

[9]A. Aviram, P. E. Seiden, and M. A. Ratner, in Ref. 2, p. 5.

[10]R. C. Haddon and F. H. Stillinger, in Ref. 2, p. 19.

[11]J. M. Warman *et al.*, Nature **320**, 615 (1986).

[12]J. M. Warman *et al.*, Chem. Phys. Lett. **128**, 95 (1986).

[13]L. T. Calcaterra, G. L. Closs, and J. R. Miller, J. Am. Chem. Soc. **105**, 670 (1983).

[14]W. G. Teich, K. Oberymayer, and G. Mahler, following paper, Phys. Rev. B **37**, 8111 (1988).

[15]G. Castro, D. Haarer, R. M. Macfarlane, and H. P. Trommersdorff, U. S. Patent No. 4,101,976 (July 18, 1978).

[16]G. C. Bjorklund, W. Lenth, and C. Ortiz, Proc. Soc. Photo-Opt. Instrum. Eng. **298**, 107 (1981).

[17]W. E. Moerner and M. D. Levenson, J. Opt. Soc. Am. **B2**, 915 (1985).

[18]K. Obermayer, G. Mahler, and H. Haken, Phys. Rev. Lett. **58**, 1792 (1987).

[19]G. Mahler and K. Obermayer, in *Computational Systems—Natural and Artificial,* Proceedings of the International Symposium on Synergetics, Schloss Elmau, Bavaria, 1987, edited by H. Haken (Springer-Verlag, Berlin, 1987).

[20]J. Maddox, Nature **327**, 97 (1987).

[21]R. Landauer, Found. Phys. **16**, 551 (1986).

[22]R. Landauer and M. Buettiker, Phys. Scr. **T9**, 155 (1985).

[23]D. Deutsch, Proc. R. Soc. London, Ser. A **400**, 97 (1985).

[24]P. Benioff, J. Stat. Phys. **29**, 515 (1982).

[25]W. H. Zurek, Phys. Rev. Lett. **53**, 391 (1984).

[26]A. Peres, Phys. Rev. A **32**, 3266 (1985).

[27]C. H. Bennett, Int. J. Theor. Phys. **21**, 905 (1982).

[28]C. H. Bennett, IBM J. Res. Dev. **17**, 525 (1973).

[29]M. Altarelli, in *Heterojunctions and Semiconductor Superlattices,* Proceedings of the Winter School, Les Houches, France, 1985, edited by G. Allen, G. Bastard, N. Boccara, M. Lannoo, and M. Voos (Springer-Verlag, Berlin, 1986), p. 12.

[30]M. Asada, Y. Miyamoto, and Y. Suematsu, IEEE J. Quantum Electron **QE - 22**, 1915 (1986).

[31]H. Haken, *Light* (North-Holland, Amsterdam, 1981), Vol. 1.

[32]B. R. Nag, *Electron Transport in Compound Semiconductors,* Vol. 11 of *Springer Series in Solid-State Sciences,* edited by H.-J. Queisser (Springer-Verlag, Berlin, 1980).

[33]S. Adachi, J. Appl. Phys. **58**, R1 (1985).

[34]M. Asada and Y. Suematsu, IEEE J. Quantum Electron **QE - 21**, 434 (1985).

[35]R. C. Miller, A. C. Gossard, D. A. Kleinman, and O. Monteanu, Phys. Rev. B **29**, 3740 (1984).

[36]R. Dingle, in *Festkörperprobleme,* edited by H.-J. Queisser (Vieweg, Braunschweig, 1975), Vol. 15. p. 21.

[37]W. Pötz and D. K. Ferry, Phys. Rev. B **32**, 3863 (1985).

[38]H. Grabert, *Projection Operator Techniques in Nonequilibrium Statistical Mechanics,* Vol. 95 of *Springer Tracts in Modern Physics,* edited by G. Höhler (Springer-Verlag, Berlin, 1982), p. 69.

[39]W. Ebeling and R. Feistel, *Physik der Selbstorganisation und Evolution* (Akademie-Verlag, Berlin, 1982), p. 303.

[40]R. Lassnig, Phys. Rev. B **31**, 8076 (1985).

[41]W. Nagourney, J. Sandberg, and H. Dehmelt, Phys. Rev. Lett. **56**, 2797 (1986).

[42]B. J. Dalton and P. L. Knight, J. Phys. **B15**, 3997 (1982).

[43]N. N. Bogolubov, Fam Le Kien, and A. S. Shumovsky, Phys. Lett. **107A**, 173 (1985).

[44]G. Bastard, Phys. Rev. B **24**, 5693 (1981).

[45]E. O. Kane, J. Phys. Chem. Solids **1**, 249 (1957).

[46]G. Bastard, Phys. Rev. B **25**, 7584 (1982).

[47]B. K. Ridley, J. Phys. C **15**, 5899 (1982).